PROTEINS
STRUCTURE ■ FUNCTION ■ BIOINFORMATICS

Solution structures of chicken parvalbumin 3 in the Ca^{2+}-free and Ca^{2+}-bound states

Michael T. Henzl,[1]* John J. Tanner,[1,2] and Anmin Tan[1]

[1] Department of Biochemistry, University of Missouri, Columbia, Missouri 65211
[2] Department of Chemistry, University of Missouri, Columbia, Missouri 65211

ABSTRACT

Birds express two β-parvalbumin isoforms, parvalbumin 3 and avian thymic hormone (ATH). Parvalbumin 3 from chicken (CPV3) is identical to rat β-parvalbumin (β-PV) at 75 of 108 residues. CPV3 displays intermediate Ca^{2+} affinity—higher than that of rat β-parvalbumin, but lower than that of ATH. As in rat β-PV, the attenuation of affinity is associated primarily with the CD site (residues 41–70), rather than the EF site (residues 80–108). Structural data for rat α- and β-parvalbumins suggest that divalent ion affinity is correlated with the similarity of the unliganded and Ca^{2+}-bound conformations. We herein present a comparison of the solution structures of Ca^{2+}-free and Ca^{2+}-bound CPV3. Although the structures are generally similar, the conformations of residues 47 to 50 differ markedly in the two protein forms. These residues are located in the C helix, proximal to the CD binding loop. In response to Ca^{2+} removal, F47 experiences much greater solvent accessibility. The side-chain of R48 assumes a position between the C and D helices, adjacent to R69. Significantly, I49 adopts an interior position in the unliganded protein that allows association with the side-chain of L50. Concomitantly, the realignment of F66 and F70 facilitates their interaction with I49 and reduces their contact with residues in the N-terminal AB domain. This reorganization of the hydrophobic core, although less profound, is nevertheless reminiscent of that observed in rat β-PV. The results lend further support to the idea that Ca^{2+} affinity correlates with the structural similarity of the apo- and bound parvalbumin conformations.

Proteins 2011; 79:752–764.

Key words: Ca^{2+}-binding protein; EF-hand protein; NMR; protein structure; protein-ligand interaction.

INTRODUCTION

Members of the EF-hand protein family participate in diverse Ca^{2+}-signaling pathways,[1–4] either as explicit regulatory proteins or as mobile Ca^{2+} buffers. The proteins are named for their distinctive helix-loop-helix Ca^{2+}-binding motif, the configuration of which can be mimicked with the thumb and first two fingers of the right hand.[5]

Despite the similarity of their metal ion-binding sites, EF-hand proteins exhibit major differences in divalent ion affinity. We are studying the physical basis for these differences in specific members of the parvalbumin family. Parvalbumins are small (M_r 12,000), vertebrate-specific EF-hand proteins[3,6,7] that are believed to function primarily as cytosolic Ca^{2+} buffers. They can be assigned to α- and β sub-lineages on the basis of isoelectric point (pI $<$ 5 for β) and lineage-specific sequence differences.[8,9] In saline at pH 7.4, the overall $\Delta G^{\circ\prime}$ for Ca^{2+} binding ranges between −18.4 and −22.3 kcal/mol. Besides improving our understanding of this biologically important EF-hand protein family, an explanation for the differences in binding affinity could furnish insight into protein-ligand interactions in general.

The PDB contains high-resolution structures for several Ca^{2+}-bound parvalbumins, including carp β (5CPV),[10] leopard-shark α (5PAL),[11] pike β (2PVB),[12] rat α (1RWY),[13,14] and rat β (1RRO).[15] Their striking similarity, irrespective of divalent ion-binding behavior, suggests that alterations in divalent ion affinity might arise from structural differences in the apo-proteins. Structural data for Ca^{2+}-free rat α- and β-parvalbumins[16,17] are consistent with this hypothesis. Whereas the unliganded- and bound states of the high-affinity α isoform are quite similar, Ca^{2+} removal is accompanied by a substantial conforma-

Additional Supporting Information may be found in the online version of this article.

Abbreviations: ANS, 8-anilinonaphthalene-1-sulfonate; ATH, avian thymic hormone; CD site, parvalbumin metal ion-binding site flanked by the C and D helices; CPV3, chicken parvalbumin 3; DSS, sodium 2,2-dimethyl-2-silapentane-5-sulfonate; EDTA, ethylenediaminetetraacetic acid; EF site, parvalbumin metal ion-binding site flanked by the E and F helices; HSQC, heteronuclear single-quantum coherence; Mes, 2-(*N*-morpholino)ethanesulfonic acid; NMR, nuclear magnetic resonance; NOE, nuclear Overhauser effect; NOESY, NOE spectroscopy; PV, parvalbumin; R_1, longitudinal relaxation rate ($1/T_1$); R_2, transverse relaxation rate ($1/T_2$); RMSD, root-mean-square-difference; S^2, generalized Lipari-Szabo order parameter; SASA, solvent-accessible surface area; TALOS, torsion angle likelihood obtained from shifts and sequence similarity; τ_c, overall rotational correlation time; τ_e, internal correlation time; R_{ex}, rate constant for μs/ms motion resulting from chemical or conformational exchange.

Grant sponsor: NSF; Grant numbers: MCB0543476 (to M.T.H. and J.J.T.), DBI-0070359; Grant sponsor: NIH; Grant number: R01 GM57289; Grant sponsor: MU Research Board
*Correspondence to: Michael T. Henzl, Department of Biochemistry, 117 Schweitzer Hall, University of Missouri, Columbia, MO 65211. E-mail: henzlm@missouri.edu.
Received 31 May 2010; Revised 29 September 2010; Accepted 7 October 2010
Published online 19 October 2010 in Wiley Online Library (wileyonlinelibrary.com).
DOI: 10.1002/prot.22915

```
        1         10         20         30         40         50
CPV3    SLTDILSPSDIAAALRDCQAPDSFSPKKFFQISGMSKKSSSQLKEIFRILDNDQ
RAT β   -I-----AE------QE--D--T-E-Q----T--L--M-A--V-D---FI----

              60         70         80         90         100
CPV3    SGFIEEDELKYFLQRFESGARVLTASETKTFLAAADHDGDGKIGAEEFQEMVQS
RAT β   --YLDG--------K-Q-D--E--E----SLMD---N--------D------H-
```

Figure 1

The amino acid sequences of CPV3-C72S[18] and rat β-PV.[19] Dashes are used to denote sequence identities.

tional change in the low-affinity β isoform—implying that the attenuated divalent ion affinity of the latter may reflect the energetic cost associated with remodeling the apo-protein.

Chicken parvalbumin 3 (CPV3) is one of two β-PV isoforms expressed in the chicken; the other is called avian thymic hormone (ATH). The sequence of CPV3 is noteworthy for its similarity to that of rat β-PV, with identities at 75 of 108 residues (Fig. 1). ATH and CPV3 were both originally discovered in the thymus gland[18,20,21] and evidently play an endocrine role in the avian immune systems, modulating T-cell maturation and proliferation.[22,23] However, both proteins have also been detected in alternative tissue settings—ATH in the avian retina[24] and CPV3 in hair cells of the avian auditory organ (basilar papilla).[25] Interestingly, the mammalian β isoform is likewise highly expressed in the mammalian auditory organ (organ of Corti), in the highly specialized sensory cells known as outer hair cells.[26,27] Presumably, ATH and CPV3 function as specialized Ca^{2+} buffers in the retina and basilar papilla.

The overall $\Delta G^{\circ\prime}$ for Ca^{2+} binding by CPV3, in saline at pH 7.4, is −85.8 kJ/mol (−20.5 kcal/mol),[28] intermediate between that of rat α-PV, at −93.8 kJ/mol (−22.4 kcal/mol) and rat β-PV, at −77.0 kJ/mol (−18.4 kcal/mol).[29] In light of the proposed correlation between divalent ion affinity and the similarity of the unliganded and Ca^{2+}-bound proteins, it was of some interest to examine the resemblance between the Ca^{2+}-free and Ca^{2+}-bound forms of CPV3. Due to our inability to crystallize Ca^{2+}-loaded CPV3, it proved necessary to determine the structure of the Ca^{2+}-bound protein, as well as the unliganded protein, by NMR. ^{15}N relaxation measurements are reported for both forms of the protein.

METHODS

Protein expression and purification

Because the wild-type CPV3 sequence includes a solvent-exposed cysteine at position 72, rather than the consensus serine, the protein readily forms disulfide-linked dimers and trimers in the absence of reductant. We have chosen to work with the C72S variant to avoid the experimental complications attendant to this behavior. This sequence substitution has no discernible impact on divalent ion affinity.[18,29] The CPV3-C72S coding sequence, optimized for expression in *Escherichia coli*, was purchased from Genscript (Piscataway, NJ) and cloned between the Nde I and Bam HI sites of pET11a. Bacteria harboring the resulting construct were grown at 37°C in ^{15}N- or ^{13}C,^{15}N-labeled Spectra 9 medium (Cambridge Isotope Laboratory, Andover, MA), containing ampicillin (100 μg/mL). For the production of protein fractionally labeled with ^{13}C, the culture medium contained 15% (v/v) ^{13}C,^{15}N-labeled Spectra 9 and 85% unlabeled Spectra 9. IPTG was added (to 0.25 m*M*) when the absorbance (at 600 nm) reached 0.6. The culture was harvested by centrifugation after an additional 20 h. Details of the purification—lysis, anion-exchange, and gel-filtration—are described elsewhere.[28] Each liter yielded 20 to 25 mg of protein, with purity exceeding 98%.

NMR sample preparation

To prepare the Ca^{2+}-free sample, sufficient protein to yield 0.5 mL of a 3 m*M* solution was concentrated to 5 mL by ultrafiltration, then dialyzed at 4°C for 48 h, against 4 L of 0.15*M* NaCl, 0.025*M* Hepes, 5.0 m*M* EDTA, pH 7.4. Dialysis was continued for 48 h against 0.15*M* NaCl, 0.01*M* Mes, 5.0 m*M* EDTA, pH 6.0. After adding 0.1 volume of buffer prepared in D_2O and 0.1% sodium azide, the solution was concentrated to 0.5 mL and loaded into a 5-mm Shigemi microcell (Shigemi, Inc., Allison Park, PA).

An analogous procedure was used to prepare the Ca^{2+}-bound protein, except that the protein sample was simply dialyzed for 48 h, with three changes, against 2 L of Mes-buffered saline, pH 6.0, containing 0.10 m*M* Ca^{2+}, prior to addition of D_2O and azide and concentration to 0.5 mL.

NMR spectroscopy

All NMR data were acquired at 20°C on a Varian INOVA 600 MHz spectrometer, equipped with a triple-

resonance cryoprobe. ^{1}H chemical shifts were referenced relative to DSS; ^{13}C and ^{15}N shifts were referenced indirectly, employing the ^{1}H/X frequency ratios. Data were processed with NMRPipe[30] and analyzed with Sparky.[31]

Resonance assignments

Backbone ^{13}C assignments relied on these pairs of 3D experiments: HNCA[32] and HN(CO)CA[33]; HNCACB[34,35] and CBCA(CO)NH[36]; and HNCO[32] and HCACO-CANH.[37] The CCONH[38] spectrum provided aliphatic ^{13}C assignments beyond C$^{\beta}$. Aliphatic ^{1}H signals were assigned with data from the HBHACONH, HCCONH,[38] ^{15}N-edited TOCSY-HSQC,[39] and HCCH-TOCSY[40] experiments. The HBCBCGCDHD and HBCBCGCDCEHE spectra[41] permitted assignment of the C$^{\delta}$ and C$^{\varepsilon}$ resonances from phenylalanine and tyrosine. Analysis of a fractionally ^{13}C-labeled sample as described by Neri *et al.*[42] yielded stereospecific assignments for the methyl protons in valine and leucine. Assignment of the ε-methyl protons of M35 were made on the basis of strong NOEs to the γ-methyl protons of V106, after initial structure calculations indicated intimate contact between the two methyl groups.

Solution structure calculations

NOE-based distance restraints were collected from three-dimensional ^{15}N-edited and ^{13}C-edited NOESY-HSQC[43] data sets acquired on ^{13}C, ^{15}N-labeled protein, employing mixing times of 125 ms and 100 ms, respectively. Cross peaks were picked manually and integrated in Sparky. TALOS[44] was used to collect ϕ,ψ dihedral angle restraints for apo- and Ca^{2+}-bound CPV. Structure calculations were performed with CYANA v. 2.1,[45] allowing the program to make all NOE assignments. CYANA combines the CANDID algorithm for iterative assignment of distance restraints with DYANA, a fast torsion-angle dynamics algorithm.[46]

To explicitly include Ca^{2+} in the structure calculations, a modified aspartate (Asm)—having Ca^{2+} covalently bound to atom OD1—was added to the standard CYANA residue library. The $+x$ ligand (D51) in the CD site of rat α-PV (PDB code 1RWY) was used to model the Asm side-chain conformation and Ca^{2+}-OD1 bond length. D51 and D90 of CPV3 were replaced with Asm residues in the CPV3 sequence input file. The remaining Ca^{2+}-O bonds in the CD site were created with link statements—connecting the Ca^{2+} of Asm51 to the appropriate O atoms of D53 (OD1), S55 (OG), F57 (O), E59 (OE1), and E62 (OE1, OE2). The corresponding bonds in the EF site were similarly defined with link statements connecting the Ca^{2+} of Asm90 to D92 (OD1), D94 (OD1), K96 (O), and E101 (OE1, OE2). Lower- and upper limits were set for these Ca^{2+}-O bonds, at 0.1 Å below and 0.1 Å above the corresponding bond lengths in the 1RWY structure. These restraints were weighted empirically, employing a value of 5.0 in the final calculation. Upper limits (3.0 Å) were also placed on the distances between Asm51 OD1 and the other O ligands in the CD site and between Asm90 OD1 and the other O ligands in the EF site. These restraints, which prevent close O-O contacts from developing as the Ca^{2+}-binding site forms, were also weighted empirically, with a value of 4.0 employed in the final calculation.

Güntert[45] has listed six criteria that a successful CYANA calculation should satisfy. The average CYANA target function should be less than 250 Å^2 in the first cycle and less than 10 Å^2 in the final cycle. The calculation should leave fewer than 20% of the cross-peaks unassigned, and 80% or more of the long-range NOEs should be retained. The RMSD for the ensemble should be under 3 Å in cycle 1, and the RMSD for the mean structures from the first and last cycles should likewise be less than 3 Å. The ensembles calculated for the Ca^{2+}-free and Ca^{2+}-bound CPV3 structures both met these criteria. The quality of the final structures was also analyzed with PROCHECK[47] and the PDB validation server.

^{15}N relaxation data

R_1, R_2, and $\{^{1}H\}^{15}N$ NOE data were collected on ^{15}N-labeled protein using Varian BioPack pulse sequences. The R_1 data were acquired with these relaxation delays, in ms: 50, 100, 150, 250, 350, 450, 600, 800, 1000, and 1200. The R_2 data were collected with delays of 10, 30, 50, 70, 90, 110, 130, 150, 170, and 190 ms. Uncertainties were estimated from replicate data sets collected at three delay values. For calculation of the steady-state heteronuclear $\{^{1}H\}^{15}N$-NOE, HSQC spectra were collected with and without 3.0 s proton saturation, employing a total recycle delay period of 5.0 s. Duplicate experiments furnished estimates of the experimental uncertainty.

Signal intensities were measured automatically for resolved amide signals in Sparky. R_1 and R_2 values were extracted by fitting the intensity data (in Origin, v. 7.5) to the equation for a two-parameter single-exponential decay. The ratio of the signal intensities in the presence and absence of proton saturation yielded an estimate for the NOE.

Analysis of the relaxation data was performed with Tensor2.[48] An overall rotational correlation time (τ_c) was estimated from a subset of amide vectors having R_2/R_1 values within one standard deviation of the mean value.[49] Internal mobilities were examined with the Lipari-Szabo model-free formalism.[50,51] Tensor2 employs the five models suggested by Clore *et al.*[52,53] and the model selection strategy described by Mandel *et al.*[54]

Accession numbers

Coordinates and structural restraints for Ca^{2+}-free CPV3 have been deposited in the Protein Data Bank with accession number 2KYC. ^{1}H, ^{15}N, and ^{13}C assignments have been deposited in the BioMagnetic Resonance Bank with accession number 16945. The corresponding

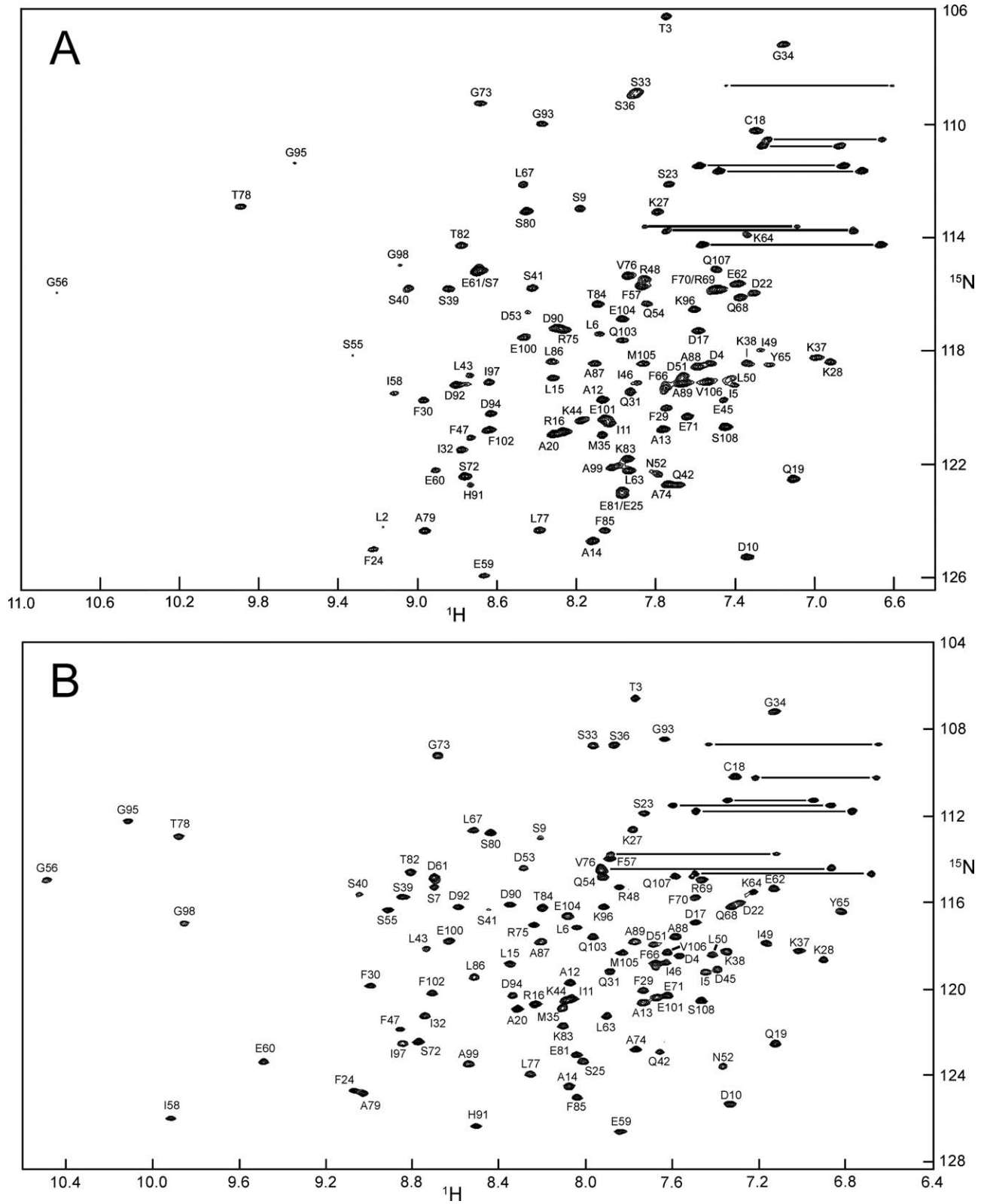

Figure 2

(**A**) ^{1}H-^{15}N HSQC spectrum of Ca^{2+}-free chicken CPV3 (3 m*M*) in 0.15*M* NaCl, 0.01*M* Mes, 0.005*M* EDTA, pH 6.0, at 20°C. (**B**) ^{1}H-^{15}N HSQC spectrum of Ca^{2+}-bound chicken CPV3 in 0.15*M* NaCl, 0.01*M* Mes, 0.1 m*M* Ca^{2+}, pH 6.0, at 20°C.

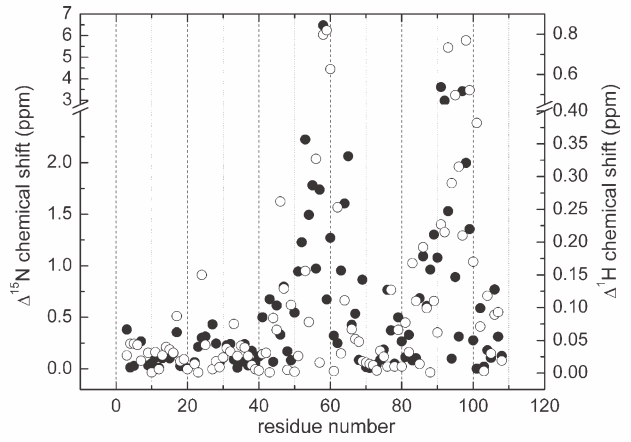

Figure 3

Chemical shift perturbations in response to Ca^{2+} binding/dissociation. The filled circles represent the absolute value of the difference in ^{15}N chemical shift; the hollow circles represent the absolute value of the difference in ^{1}H chemical shift.

accession numbers for the Ca^{2+}-bound protein are 2KYF and 16955, respectively.

RESULTS

Resonance assignments

The CBCACONH and HNCACB spectra yielded assignments for the C^{α} and C^{β} nuclei. The HNCA/HNCOCA and HNCO/HCACOCANH spectral pairs were used to confirm the backbone assignments and to resolve ambiguities. Aliphatic carbon assignments beyond C^{β} were made with the CCONH experiment. The aliphatic side-chain carbon assignments were complete, excluding the 18 carboxylates (Asp, Glu, and C-terminus), the seven carboxamides (5 Gln, 2 Asn), and the R75 guanidinino group.

Aliphatic ^{1}H assignments were made from HBHACONH, HCCONH, ^{15}N-edited TOCSY-HSQC, and HCCH-TOCSY experiments. Assignments for H^{δ} and H^{ε} in Phe and Tyr were obtained from the HBCBCGCDHD and HBCBCGCDCEHE experiments, which correlate those protons with C^{β}. Proton assignments were greater than 95% complete for both the Ca^{2+}-free and Ca^{2+}-bound forms of the protein.

Figure 2(A) displays the ^{1}H-^{15}N HSQC spectrum of Ca^{2+}-free CPV3 at 20°C. Signals are observed for each of the main-chain amide signals. The following pairs of resonances are strongly overlapped: S7/E61, I11/E101, R16/A20, E25/E81, S33/S36, Q42/A74, R48/F57, D51/A89, R69/F70, and R75/D90.

The ^{1}H-^{15}N HSQC spectrum of Ca^{2+}-bound CPV3 at 20°C is displayed in Figure 2(B). Main-chain amide signals are observed for all residues except I2. The spectrum exhibits improved dispersion relative to that of the Ca^{2+}-free protein, with major overlap restricted to just three pairs of resonances: I11/K44, D22/Q68, and Q54/V76. Figure 3 displays the backbone amide ^{1}H and ^{15}N chemical shift differences produced by Ca^{2+} binding for each amide signal. The superimposed spectra for the apo- and Ca^{2+}-bound protein are displayed in Supporting Information, Figure 1.

Solution structure of Ca^{2+}-free CPV3

Figure 4(a) displays an ensemble of 20 low-energy conformers of Ca^{2+}-free CPV3 calculated with CYANA.[45] The calculation employed 1937 distance restraints collected from ^{15}N- and ^{13}C-edited NOESY-HSQC spectra, as well as 158 dihedral angle restraints generated with TALOS.

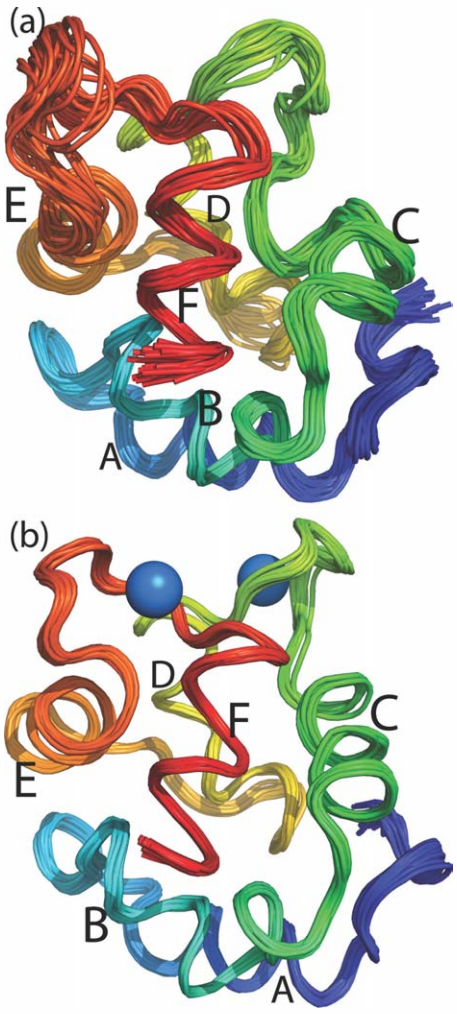

Figure 4

Tertiary structure of CPV3. (**a**) Solution structure of Ca^{2+}-free CPV3. An ensemble of 20 low-energy structures calculated with CYANA. (**b**) Low-energy ensemble of Ca^{2+}-bound CPV3. The spheres represent the average position of the Ca^{2+} ions in the ensemble. This and Figures 8 to 10 were produced with PyMol.[55]

Table I
Restraints and Statistical Analysis for Ca^{2+}-Free and Ca^{2+}-Bound CPV3 Structures

	Ca^{2+}-free CPV3	Ca^{2+}-bound CPV3
No. experimental restraints		
Total NOEs	1937	2825
Intraresidue	528	655
Sequential	532	682
Medium-range ($1 < \|i - j\| \leq 4$)	448	684
Long-range ($\|i - j\| > 4$)	429	804
TALOS	158	171
Residual CYANA target function	2.34 ± 0.25	6.20 ± 0.42
Restraint violations		
NOE restraints (>0.1 Å, 6 or more structures)	8	42
NOE restraints (>0.2 Å, 6 or more structures)	2	13
NOE restraints (>0.3 Å, 6 or more structures)	1	3
NOE restraints (>0.4 Å, 6 or more structures)	1	1
Dihedral restraints (>5°, 6 or more structures)	0	2
RMSD from experimental restraints		
NOE restraints (Å)	0.019 ± 0.002	0.029 ± 0.002
Dihedral restraints (deg.)	0.66 ± 0.21	1.34 ± 0.15
RMSD from idealized covalent geometry		
(values in parentheses include hydrogen atoms)		
Bonds (Å)	0.0019 (0.0095)	0.0043 (0.010)
angles (deg)	0.29 (0.56)	1.1 (0.87)
Dihedral angles (deg)	25.7	28.3
Improper angles (deg)	0.089 (0.31)	0.087 (0.30)
Coordinate RMSD from average structure (Å)		
Backbone (C^{β}, C^{α},C′,O, N)	0.66 ± 0.13	0.30 ± 0.06
All heavy atoms	1.07 ± 0.13	0.67 ± 0.07
Ramachandran plot (ensemble averages)		
Most favored regions (%)	64.3	75.3
Allowed regions (%)	34.8	24.6
Generously allowed (%)	0.9	0.0
Disallowed (%)	0.0	0.1

Table I lists structural quality statistics for the ensemble. The RMSD, relative to the ensemble average, is 0.66 Å for the backbone atoms (C^{β}, C^{α}, C′, O, and N), 1.07 Å for all heavy atoms. 100% of the ϕ,ψ combinations in the 20 conformers reside in favored, allowed, or generously allowed regions of the Ramachandran plot. The average NOE restraint violation is 0.019 Å, and there is just one violation exceeding 0.4 Å in six or more of the structures. The average dihedral restraint violation is 0.66°, with no violations exceeding 5° in six or more structures.

Solution structure of Ca^{2+}-bound CPV3

CYANA was likewise used to determine the tertiary structure of Ca^{2+}-bound CPV3. Interestingly, the ^{15}N- and ^{13}C-edited NOESY experiments yielded substantially more crosspeaks than the corresponding experiments on the apo-protein, despite the fact that the sample concentrations were comparable. Thus, the calculation on the Ca^{2+}-loaded protein utilized 2825 distance restraints and 171 TALOS restraints. Given that the backbone dynamics for the two protein forms are not radically different (vide infra), the disparate number of NOEs presumably reflects greater sidechain motion in the apo-protein.

The resulting ensemble of 20 low-energy Ca^{2+}-bound conformers is displayed in Figure 4(b). The RMSD for the ensemble is 0.30 Å for backbone atoms and 0.67 Å for all heavy atoms. With the exception of I2 in one of the conformers, all ϕ,ψ combinations reside in allowed regions of the Ramachandran plot. The average NOE restraint violation is 0.029 Å, with just one violation in excess of 0.4 Å in six or more structures. The average dihedral restraint violation is 1.34°, with just two violations exceeding 5° in six or more structures.

Comparison of the Ca^{2+}-bound and Ca^{2+}-free CPV3 structures

An average RMSD of 2.27 ± 0.08 Å was calculated for corresponding C^{α} atoms in the Ca^{2+}-bound and Ca^{2+}-free structures. This value was obtained by averaging over all pairs of conformers in the two ensembles. The values observed for individual conformer pairs ranged from 2.02 to 2.48 Å. RMSD values for the ensemble-averaged Ca^{2+}-free and Ca^{2+}-bound structures are plotted as a function of residue number in Figure 5. *A priori*, large differences are anticipated in the ion-binding loops, where the presence or absence of the divalent ion is expected to impact the path of the polypeptide chain. In fact, elevated RMSDs are observed for residues 51 to 55

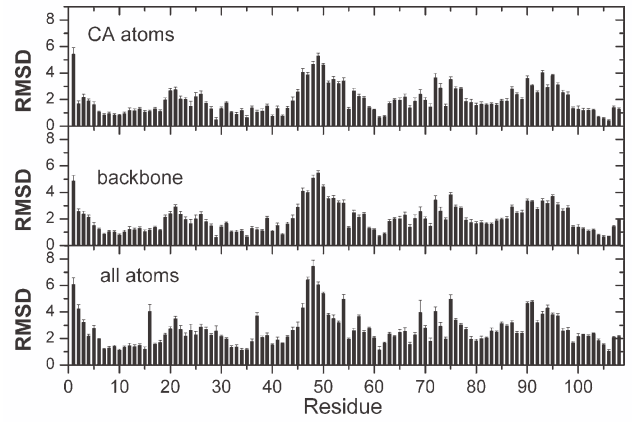

Figure 5

The RMSD values (in Å) between the Ca^{2+}-free and Ca^{2+}-bound structures of CPV3 have been plotted as a function of residue number. (top) RMSD for the C^{α} atoms; (middle) the average RMSD for all of the backbone atoms; (bottom) average RMSD average for all atoms in the residue. The RMSD values were averaged over all possible pairwise combinations of the 20 chains in the Ca^{2+}-free and Ca^{2+}-bound ensembles, using CNS.[56] The error bars represent one standard deviation.

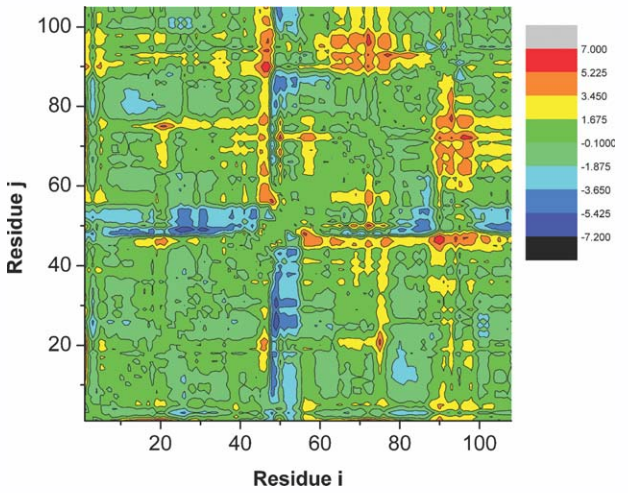

Figure 6

Difference distance map. The changes in inter-residue distance (in Å) that accompany Ca^{2+} removal were calculated with CNS. The quantity r_{ij} (Ca^{2+}-free)—r_{ij}(Ca^{2+}-bound) is displayed as a contour plot, where r_{ij}(Ca^{2+}-free) is the C_{α}-C_{α} distance for residues i and j in the Ca^{2+}-free structure, and r_{ij}(Ca^{2+}-bound) is the corresponding distance for the Ca^{2+}-bound structure. The differences were averaged over all possible combinations of the 20 chains in the Ca^{2+}-free and Ca^{2+}-bound ensembles.

in the CD loop and for residues 90 to 96 in the EF loop. Significantly elevated values are also observed in several other regions of the molecule. These include residues 19 to 23 in the AB loop, residues 46 to 50 in the C-terminal half of helix C, and residues 65 to 78, corresponding to the C-terminal half of the D-helix and the extended D/E loop.

Figure 6 compares the Ca^{2+}-bound and Ca^{2+}-free structures using a difference distance map, in which the inter-residue distance between pairs of C^{α} atoms in the Ca^{2+}-bound CPV3 structure has been subtracted from the corresponding distance in the Ca^{2+}-free structure. Distances that increase with Ca^{2+} removal are displayed in red, whereas distances that decrease in the absence of Ca^{2+} are displayed in blue. The C^{α} atoms in residues 47 to 57 evidently adopt positions closer to the AB domain (residues 1–40), but further from residues 60 to 108 in the apo-form of the protein. Also, upon dissociation of Ca^{2+}, the C^{α} atoms in the EF loop (90–100) occupy positions more distant from their counterparts in the D and E helices and in the extended D/E loop.

Figure 7 displays the changes in solvent-accessible surface area (SASA) that accompany Ca^{2+}-removal, as a function of residue number. F47, R48, and I49 exhibit the largest values, followed by R69 and R75. Marginally increased accessibility is also observed for D90 and T3. Given the substantial rearrangement of the EF site ion-binding loop upon Ca^{2+} removal, the heightened accessibility of D90 (the -x ligand) is probably meaningful. However, the significance of the increased SASA of T3 is questionable, considering its proximity to the N-terminus, where the ensembles exhibit increased disorder.

Figure 8 presents a stereoview of the superimposed, ensemble-averaged apo- (magenta) and Ca^{2+}-bound (green) CPV3 structures, highlighting several residues at the C-terminal end of helix C. Arguably, the most inter-

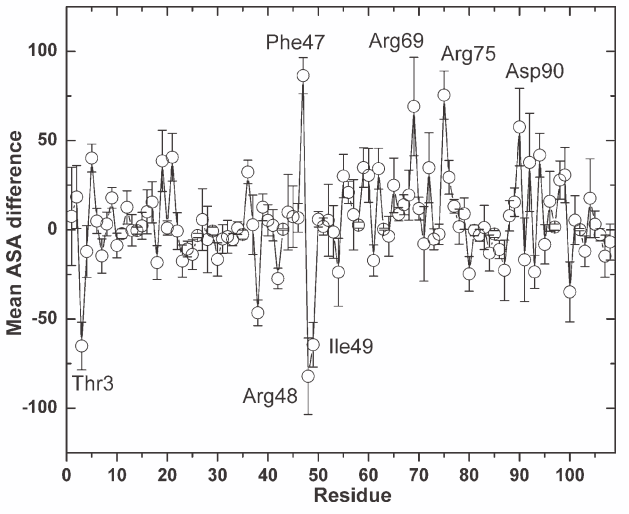

Figure 7

Estimated changes in solvent-accessible surface area that accompany Ca^{2+} removal from CPV3. Each point represents the accessible surface area of a residue in the Ca^{2+}-free conformation minus that of the corresponding residue in the Ca^{2+}-bound conformation, averaged over all possible pairwise combinations of the 20 chains in each ensemble. The error bars represent one standard deviation.

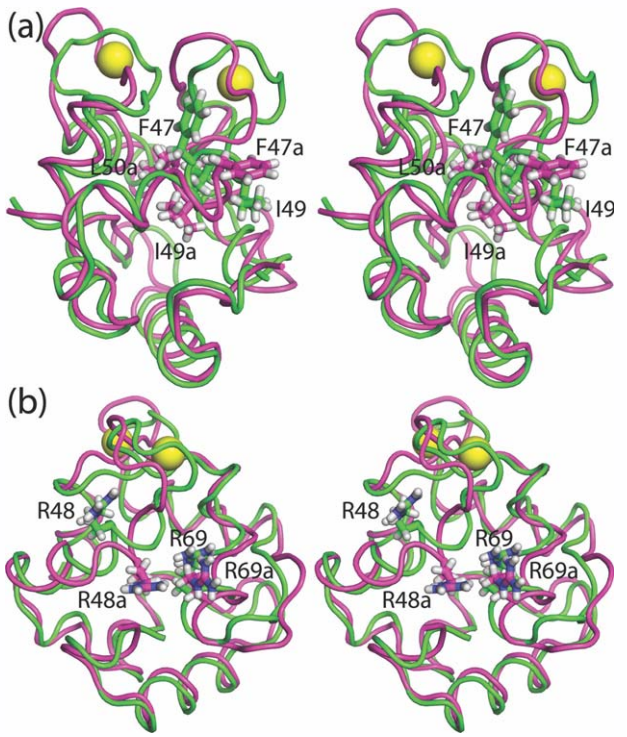

Figure 8

Stereoviews of the superimposed ensemble-averaged structures of Ca^{2+}-bound (green) and Ca^{2+}-free (magenta) CPV3. The side-chains of F47, R48, I49, and L50 are included to emphasize the extent of their realignment. The apo-protein residues are indicated by the letter "a" appended to the residue label. (**b**) Represents an approximately 90° rotation of view (**a**). The sidechain of (Ca^{2+}-bound) L50 is obscured in (a) and was left unlabeled.

esting conformational alterations are observed in this region of the molecule, proximal to the CD binding site. Ca^{2+} removal is apparently accompanied by a partial reconfiguration of the hydrophobic core. Whereas the side-chain of F47 is largely buried in the Ca^{2+}-loaded state, it becomes much more solvent-accessible upon dissociation of the divalent ion [Fig. 8(a)]. By contrast, I49 enjoys substantial solvent accessibility in the Ca^{2+}-bound state, but adopts an interior position in the apo-protein. Although the accessibility of L50 is unchanged, the residue undergoes reorientation, facilitating contact with I49. The side-chain of R48 also relocates upon Ca^{2+} removal, adopting a position in the cleft between the C and D helices, adjacent to R69 [Fig. 8(b)]. The coordinated movement R48 and R69 substantially reduces the solvent accessibility of R48, while increasing the accessibility of R69.

Figure 9 presents a close-up stereoview of the ligation-dependent changes in the vicinity of F47, I49, and L50. The configuration of these residues in the Ca^{2+}-free protein is displayed in panel (a); the corresponding view of the Ca^{2+}-loaded protein is shown in Figure 9(b). Whereas only the edge of F47 has significant surface exposure when Ca^{2+} is bound, the entire phenyl ring becomes accessible in the apo-protein. The side-chain of I49 is largely exposed in the Ca^{2+}-bound protein, but becomes completely sequestered upon Ca^{2+} removal. Whereas the side-chain of L50 is completely buried in the Ca^{2+}-bound protein, the side-chain experiences minor exposure in the Ca^{2+}-free protein.

The orientations of F66 and F70 change perceptibly upon dissociation of Ca^{2+}. In the Ca^{2+}-bound protein [Fig. 10(b)], the phenyl rings are intimately associated with residues from the AB domain, notably F29. Although F66 contacts one of the methyl groups in L50, interaction with I49 and L50 is otherwise minimal. With the removal of Ca^{2+}, F66 and F70 approach the side-chains I49 and L50 [Fig. 10(a)]. The phenyl ring of F29 likewise undergoes repositioning, perhaps to retain contact with F66 and F70. Earlier, we noted the elevated RMSD values observed for residues 65 to 78, which reside in the C-terminal half of helix D and the extended D/E loop. The reorientation of F66 and F70, in concert with that of R69, may provoke the repositioning of the

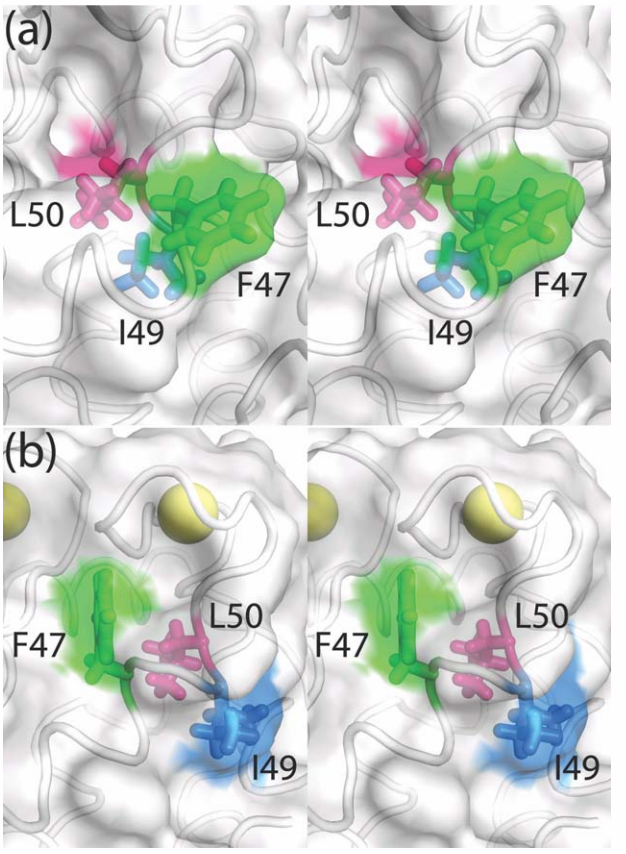

Figure 9

Stereoviews of the ligation-dependent reorientation of F47, I49, and L50 in Ca^{2+}-free (**a**) and Ca^{2+}-bound (**b**) forms of CPV3.

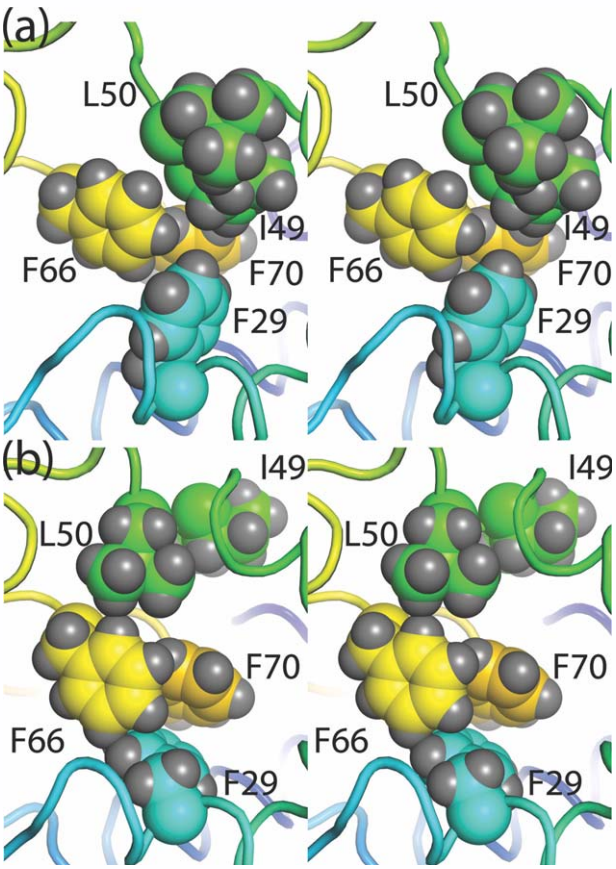

Figure 10

Stereoviews of the ligation-dependent orientation of F66 and F70 in Ca^{2+}-free (**a**) and Ca^{2+}-bound (**b**) forms of CPV3.

polypeptide backbone in the D/E region, resulting in the heightened RMSD values observed for residues 72 to 78.

^{15}N relaxation analysis

Ca^{2+}-free CPV3

Relaxation data were collected at 20°C. The R_1 and R_2 data are well accommodated by a two-parameter exponential decay model. Resonances having substantial overlap were omitted from the analysis. R_1 and R_2 values for 83 of 107 amide vectors are plotted in Figures 11(A,B), respectively. The corresponding numerical values are tabulated in Supporting Information, Table I. Resonances having substantial overlap were omitted from the analysis.

The rotational correlation time (τ_c) was estimated from the subset of amide vectors [Fig. 11(C), •] having an R_2/R_1 ratio within one standard deviation of the mean. The data are well accommodated by a spherically symmetric rotational diffusion model, yielding a τ_c value of 6.92 ± 0.04 ns, which corresponds to a rotational diffusion coefficient of 2.41×10^7 s^{-1}. Axially symmetric and fully symmetric models yielded insignificant reductions in χ^2. The ensemble-averaged apo-protein structure exposes 6080 Å^2 of total surface area, as determined with Naccess.[57] Substituting this value into the empirical relationship between τ_c and total SASA derived by Krishnan and Cosman[58] affords a predicted τ_c of 6.76 ns, which agrees well with the τ_c estimate obtained from the trimmed R_2/R_1 values.

The $\{^1H\}^{15}N$ NOE values [Fig. 11(D)] are tightly clustered about a mean value of 0.81 ± 0.06. Only seven amides exhibit values below 0.75. These include T3 (0.70); N52 (0.71) and D53 (0.73) in the CD binding loop; D92 (0.71) and G93 (0.72) in the EF binding loop; and the C-terminal S108 (0.48).

Main-chain flexibility was examined using the Lipari-Szabo treatment.[50,51] Relaxation data for 73 of the 83 amide vectors were amenable to treatment using the model-free approach, employing a spherically symmetric

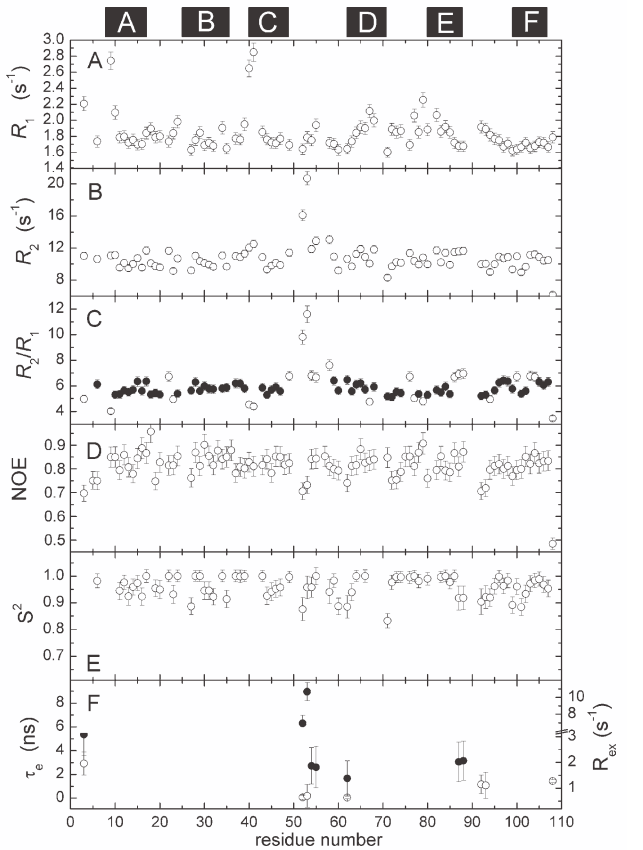

Figure 11

^{15}N relaxation data and internal mobility analysis for Ca^{2+}-free CPV3. The approximate positions of the six helical segments are indicated at the top of the figure. (**A**) R_1 values. (**B**) R_2 values. (**C**) Calculated R_2/R_1 ratios. The filled circles (●) represent the amide vectors used in the estimation of τ_c. (**D**) $\{^1H\}^{15}N$ NOE values. (**E**) Order parameter (S^2) determined by model-free analysis. (**F**) τ_e (○) and R_{ex} (●) values for residues displaying motion on a timescale exceeding 20 ps.

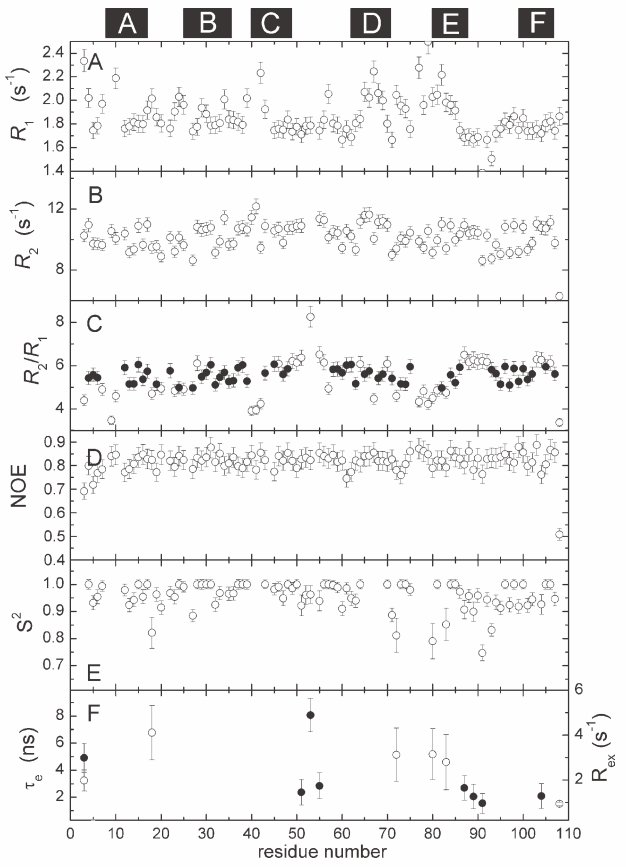

Figure 12

^{15}N relaxation analysis of Ca^{2+}-bound CPV3. (**A**) R_1 values. (**B**) R_2 values. (**C**) R_2/R_1 ratios, the filled circles denoting those amides used to estimate τ_c. (**D**) $\{^1H\}^{15}N$ NOE values. (**E**) The order parameter (S^2) obtained from model-free analysis. (*F*) τ_e (○) and R_{ex} (●) values for residues displaying lower frequency local motions.

diffusion model. The results are displayed in Figures 11(E,F), and the model-free parameters are listed in Supporting Information, Table III.

The motion of 61 amide vectors can be modeled with the overall rotational correlation time (τ_c) and a generalized order parameter (S^2). Two amides (D92, G93) require a τ_e term to describe internal motion on the 20 ps to 10 ns timescale. An additional five (Q54, S55, I58, L86, A87) require an R_{ex} term to describe internal motion on the μs-ms timescale. Four amides (D4, N52, D53, E62) can be accommodated only by inclusion of both τ_e and R_{ex} terms. Finally, residue 108 exhibits behavior consistent with motion on two timescales shorter than the overall rotational correlation time. The average order parameter for the apo-protein is 0.95, identical to the value obtained for Ca^{2+}-free ATH and comparable to the value of 0.92 obtained for the Ca^{2+}-free forms of rat α-PV and rat β-PV.[16,17,59]

The data for 10 of the 83 vectors for which relaxation data were collected are not compatible with any of the five standard models, suggesting that those amides are undergoing more complex motions. The residues in question are S9, D10, C18, S40, S41, Y65, L67, Q68, A79, and T82. Their positions are displayed in Supporting Information, Figure 2(A).

Ca^{2+}-bound CPV3

Relaxation data were likewise collected on the Ca^{2+}-bound form of the protein at 20°C. The improved dispersion of the $^1H,^{15}N$-HSQC spectrum permitted extraction of R_1 and R_2 values for 99 of the 107 amide vectors [Figs. 12(A,B), respectively]. The numerical values are tabulated in Supporting Information, Table II.

As described above, τ_c was estimated from the subset of amide vectors [Fig. 12(C), •] having an R_2/R_1 ratio within one standard deviation of the mean. A spherically symmetric rotational diffusion model yielded a τ_c of 6.78 ± 0.02 ns, corresponding to a rotational diffusion coefficient of 2.46×10^7 s^{-1}. Axially symmetric and fully anisotropic models did not afford any further reduction in χ^2. The predicted τ_c value for the ensemble-averaged Ca^{2+}-bound structure is 6.47 ns, based on the exposure of 5900 $Å^2$ of surface, estimated with Naccess.[57] Thus, as noted above for the apo-protein, the calculated and measured rotational correlation times for the Ca^{2+}-loaded protein exhibit reasonable agreement.

The $\{^1H\}^{15}N$ NOE values [Fig. 12(D)] exhibit a mean value of 0.81 ± 0.05. Only T3, (0.69), I5 (0.72), and S108 (0.51) have steady-state NOEs below 0.75.

Relaxation data for 83 of the 99 amide vectors were amenable to the Lipari-Szabo model-free treatment, employing an isotropic diffusion model. The results are displayed in Figures 12(E,F). Numerical values for the model-free parameters are tabulated in Supporting Information, Table IV.

The motions of the majority of the amide vectors (68/83) can be modeled with τ_c and S^2. Five require a τ_e term to describe internal motion on the 20 ps to 10 ns timescale (I5, C18, S72, S80, K83). Eight others require an R_{ex} term to describe internal motion on the μs-ms timescale (D51, N52, D53, S55, A87, A89, H91, E104). One amide (T3) requires the inclusion of both τ_e and R_{ex} terms, and residue 108 evidently experiences motion on two timescales shorter than the overall rotational correlation time. The average order parameter for the Ca^{2+}-bound protein, at 0.95, is virtually identical to that determined for the apo-protein.

The data for 16 of 99 amide vectors are not compatible with any of the five standard models: S7, S9, G34, S40, S41, Q42, Y65, F66, L67, Q68, R69, L77, T78, A79, T82, and Q103.

Their positions in the Ca^{2+}-bound protein are shown in Supporting Information, Figure 2(B). This list shows considerable overlap with that for the Ca^{2+}-free protein.

Only S7, G34, Q42, F66, R69, L77, and Q103 are not represented in the apo-protein list. And of those residues, data were not available for residues S7, Q42, and R69 in the Ca^{2+}-free protein.

DISCUSSION

Several years ago, the uncanny resemblance of the Ca^{2+}-loaded parvalbumin structures in the PDB prompted the collection of structural data for several unliganded parvalbumins. With this study, the solution structures of four Ca^{2+}-free parvalbumin isoforms have been obtained. Data for the (high-affinity) rat α and (low-affinity) rat β isoforms suggested that divalent ion affinity is correlated with the similarity of the unliganded and bound states of the protein.

The tertiary structure of rat α-PV is largely independent of ligation state. By contrast, in rat β-PV, Ca^{2+} binding and dissociation is accompanied by substantial rearrangement of the hydrophobic core. Whereas residues 49, 50, and 85 are closely associated in the apo-protein, the interaction is abolished when Ca^{2+} binds. This noncovalent contact, absent in the Ca^{2+}-free forms of rat α-PV or ATH, offers a rationale for the sequence eccentricities in rat β-PV. Whereas the β-parvalbumin consensus sequence includes I49, L50, and F85, rat β incorporates F49, I50, and L85 at these positions. Site-directed mutagenesis data[60] strongly suggest that the energy required to break the contact between residues 49, 50, and 85 in the apo-form of rat β-PV reduces the net binding free energy, accounting in part for the observed attenuation of divalent ion affinity. Specifically, replacement of L85 by phenylalanine significantly increases divalent ion affinity, and the magnitude of the increase is sensitive to the identity of the residues 49 and 50. The rat β sequence also departs from the parvalbumin norm at positions 57 (Y replaces F), 58 (L replaces I), 59 (D replaces E), and 60 (G replaces E), and these residues likewise influence the impact of the L85F mutation.

It should be noted that, although ATH is a high-affinity parvalbumin, the structures of unliganded and Ca^{2+}-bound structures differ perceptibly.[61] Ca^{2+} removal is accompanied by a rigid-body movement, involving rotation and displacement, of the B helix. This structural alteration exposes substantial apolar surface area and presumably explains the major increase in ANS fluorescence emission that accompanies addition of the unliganded protein, but not the Ca^{2+}-bound protein, to a solution of that hydrophobic probe.[62] Except for the modification of helix B, however, the Ca^{2+}-bound and Ca^{2+}-free structures are very similar. In contrast to the rat β isoform, the packing of the hydrophobic core is largely unperturbed. With respect to divalent ion affinity, the critical issue may be the extent to which Ca^{2+} binding and dissociation provoke restructuring of the hydrophobic core.

The sequence similarity of rat β and CPV3 (69% identity) and the intermediate Ca^{2+} affinity of the latter fostered speculation as to whether unliganded CPV3 would exhibit any suggestion of the structural alterations observed in rat β. CPV3 harbors the parvalbumin consensus residues at positions 49, 50, 57, 58, 59, 60, and 85. However, the otherwise strong sequence conservation with rat β in the AB domain and the CD site (Fig. 1) might encourage the unliganded CPV3 to adopt a structure that differed in significant respects from that of the Ca^{2+}-loaded protein.

Interestingly, Ca^{2+} dissociation provokes a significant structural alteration just proximal to the CD binding loop, involving residues 46 to 50. Much as F49 and I50 rotate into the apolar interior of rat β-PV in response to Ca^{2+} removal, I49 and L50 are similarly sequestered in apo-CPV3. Accompanying the reorientation of residues 49 and 50, the side-chain of F47 adopts a more solvent-exposed configuration. The side-chains of I49 and L50 appear to interact. Concomitant with these changes, R48 and R69 approach each other and occupy the cleft between the helix C and the C-terminal end of the helix D.

The movement of F47, I49, and L50 is accompanied by reorientation of F66 and F70. In the Ca^{2+}-bound protein, these residues interact strongly with residues in the AB domain, notably F29. With dissociation of Ca^{2+}, however, the phenyl rings assume a configuration that permits interaction with I49 and L50, as well as F29. The side-chain of F85 approaches the side-chains of I49 and L50 but does not contact those residues. It would be of interest to examine the impact of the F85L mutation on divalent ion-binding behavior—both in wild-type CPV3 and in variants harboring the I49F and/or L50I substitutions.

The reorientation of F66 and F70 in CPV3 is reminiscent of that seen upon Ca^{2+} removal from rat β-PV. In the latter, however, F66 and F70 actually withdraw from the hydrophobic core, which permits the D helix—distorted in the Ca^{2+}-bound state—to straighten. Although the orientation of helix D is largely unchanged in Ca^{2+}-free CPV3, the realignment of F66 and F70 may contribute to repositioning of the polypeptide backbone in the extended D/E loop. ^{15}N relaxation measurements suggest that the D helix and the D/E loop region comprise a very dynamic region of the molecule. Seven of the residues that experience the most complex atomic motion in both the Ca^{2+}-free and Ca^{2+}-bound structures reside this region: F66, L67, Q68, R69, L77, T78, and A79.

In rat β-PV, the departure of the unliganded conformation from the high-affinity parvalbumin norm is attributable, at least in part, to the I49F, L50I, and F85L substitutions. CPV3, however, harbors the consensus residue at each of these positions. Thus, the basis for the atypical unliganded conformation is less clear. It could possibly reflect the sequence identity between CPV3 and

rat β-PV in other regions of the molecule, notably in the AB domain. In this context, we previously examined the interaction between the AB and CD-EF domains in rat α- and β-PV, employing the individual AB and CD-EF peptides.[63] Interestingly, in the presence of saturating Ca^{2+}, the β CD-EF peptide exhibits markedly greater affinity for the α AB peptide than the β AB peptide. Similarly, an equimolar mixture of α AB and β CD-EF exhibited substantially higher affinity for Ca^{2+} than the corresponding mixture of the β peptides. These observations implied that the AB domain imposes some structural restraint on the unliganded CD-EF domain, reversal of which requires the expenditure of Ca^{2+}-binding energy.

CONCLUSIONS

Based on an admittedly small number of data points, there appears to be a correlation between the similarity of the unliganded and Ca^{2+}-bound conformations and divalent ion affinity. At one extreme, the two states of the high-affinity rat α isoform are very similar. At the other, substantial differences are observed between the structures of the low-affinity rat β isoform. In between, the conformations of the intermediate-affinity CPV3, although similar, exhibit a reorganization of the core residues that is reminiscent of that observed in rat β.

ACKNOWLEDGMENTS

The authors thank Dr. Wei Wycoff, staff NMR Spectroscopist for the MU NMR Facility, for assistance with NMR data acquisition. The Varian 600 MHz spectrometer used for this work was acquired with the assistance of NSF award DBI-0070359, NIH award R01 GM57289 (for the cryoprobe), and the MU Research Board.

REFERENCES

1. Kretsinger RH. Structure and evolution of calcium-modulated proteins. CRC Crit Rev Biochem 1980;8:119–174.
2. Kawasaki H, Kretsinger RH. Calcium-binding proteins 1: EF-hands. Protein Profile 1995;2:297–490.
3. Celio MR, Pauls T, Schwaller B. Guidebook to the calcium-binding proteins. Oxford: Oxford University Press; 1996.
4. Kawasaki H, Nakayama S, Kretsinger RH. Classification and evolution of EF-hand proteins. Biometals 1998;11:277–295.
5. Kretsinger RH, Nockolds CE. Carp muscle calcium-binding protein. II. Structure determination and general description. J Biol Chem 1973;248:3313–3326.
6. Pauls TL, Cox JA, Berchtold MW. The Ca^{2+}-binding proteins parvalbumin and oncomodulin and their genes: new structural and functional findings. Biochim Biophys Acta 1996;1306:39–54.
7. Schwaller B. The continuing disappearance of "pure" Ca^{2+} buffers. Cell Mol Life Sci 2009;66:275–300.
8. Goodman M, Pechere JF. The evolution of muscular parvalbumins investigated by the maximum parsimony method. J Mol Evol 1977;9:131–158.
9. Moncrief ND, Kretsinger RH, Goodman M. Evolution of EF-hand calcium-modulated proteins. I. Relationships based on amino acid sequences. J Mol Evol 1990;30:522–562.
10. Swain AL, Kretsinger RH, Amma EL. Restrained least squares refinement of native (calcium) and cadmium-substituted carp parvalbumin using X-ray crystallographic data at 1.6-Å resolution. J Biol Chem 1989;264:16620–16628.
11. Roquet F, Declercq JP, Tinant B, Rambaud J, Parello J. Crystal structure of the unique parvalbumin component from muscle of the leopard shark (Triakis semifasciata). The first X-ray study of an alpha-parvalbumin J Mol Biol 1992;223:705–720.
12. Declercq JP, Evrard C, Lamzin V, Parello J. Crystal structure of the EF-hand parvalbumin at atomic resolution (0.91 Å) and at low temperature (100 K). Evidence for conformational multistates within the hydrophobic core. Protein Sci 2010;8:2194–2204.
13. McPhalen CA, Sielecki AR, Santarsiero BD, James MNG. Refined crystal structure of rat parvalbumin, a mammalian α-lineage parvalbumin, at 2.0 Å resolution. J Mol Biol 1994;235:718–732.
14. Bottoms CA, Schuermann JP, Agah S, Henzl MT, Tanner JJ. Crystal structure of rat α-parvalbumin at 1.05 Å resolution. Protein Sci 2004;13:1724–1734.
15. Ahmed FR, Rose DR, Evans SV, Pippy ME, To R. Refinement of recombinant oncomodulin at 1.30 Å resolution. J Mol Biol 1993;230:1216–1224.
16. Henzl MT, Tanner JJ. Solution structure of Ca^{2+}-free rat β-parvalbumin (oncomodulin). Protein Sci 2007;16:1914–1926.
17. Henzl MT, Tanner JJ. Solution structure of the Ca^{2+}-free rat α-parvalbumin. Protein Sci 2008;17:431–438.
18. Hapak RC, Zhao H, Boschi JM, Henzl MT. Novel avian thymic parvalbumin displays high degree of sequence homology to oncomodulin. J Biol Chem 1994;269:5288–5296.
19. Gillen MF, Banville D, Rutledge RG, Narang S, Seligy VL, Whitfield JF, MacManus JP. A complete complementary DNA for the oncodevelopmental calcium-binding protein, oncomodulin. J Biol Chem 1987;262:5308–5312.
20. Barger B, Pace JL, Ragland WL. Purification and partial characterization of an avian thymic hormone. Thymus 1991;17:181–197.
21. Hapak RC, Stanley CM, Henzl MT. Intrathymic distribution of the two avian thymic parvalbumins. Exp Cell Res 1996;222:234–245.
22. Novak R, Henzl MT, Ragland WL. Receptor cells for the CPV3 parvalbumin of chicken thymus in spleen and caecal tonsils. J Allergy Clin Immunol 99:S202, 1997.
23. Novak R, Brewer JM, Ragland WL. Immunophenotype of splenic lymphocytes with receptors for avian thymic hormone. FASEB J 1996;10:A1048.
24. Rada JA, Denis CS. Analysis of gene expression during the recovery from experimental myopia. Mol Biol Cell 2003;14:367a.
25. Heller S, Bell AM, Denis CS, Choe Y, Hudspeth AJ. Parvalbumin 3 is an abundant Ca^{2+} buffer in hair cells. J Assoc Res Otolaryngol 2002;3:488–498.
26. Henzl MT, Shibasaki O, Comegys TH, Thalmann I, Thalmann R. Oncomodulin is abundant in the organ of Corti. Hear Res 1997;106:105–111.
27. Sakaguchi N, Henzl MT, Thalmann I, Thalmann R, Schulte BA. Oncomodulin is expressed exclusively by outer hair cells in the organ of Corti. J Histochem Cytochem 1998;46:29–39.
28. Henzl MT, Agah S. Divalent ion-binding properties of the two avian β-parvalbumins. Proteins 2006;62:270–278.
29. Henzl MT, Larson JD, Agah S. Influence of monovalent cations on rat α- and β-parvalbumin stabilities. Biochemistry 2000;39:5859–5867.
30. Delaglio F, Grzesiek S, Vuister GW, Zhu G, Pfeifer J, Bax A. NMRPipe: a multidimensional spectral processing system based on UNIX pipes. J Biomol NMR 1995;6:277–293.
31. Goddard TD, Kneller DG. Sparky 3, University of California, San Francisco. 2007.
32. Ikura M, Kay LE, Bax A. A novel approach for sequential assignment of ^{1}H, ^{13}C, and ^{15}N spectra of larger proteins: Heteronuclear triple-resonance three-dimensional NMR spectroscopy. Appl Calmodulin Biochem 1990;29:4659–4667.
33. Bax A, Ikura M. An efficient 3D NMR technique for correlating the proton and ^{15}N backbone amide resonances with the alpha-carbon

of the preceding residue in uniformly $^{15}N/^{13}C$ enriched proteins. J Biomol NMR 1991;1:99–104.
34. Kay LE, Xu GY, Yamazaki T. Enhanced-sensitivity triple-resonance spectroscopy with minimal H_2O saturation. J Magn Reson 1994;109: 129–133.
35. Muhandiram DR, Kay LE. Gradient-enhanced triple-resonance three-dimensional NMR experiments with improved sensitivity. J Magn Reson 1994;103:203–216.
36. Grzesiek S, Bax A. Correlating backbone amide and side chain resonances in larger proteins by multiple relayed triple resonance NMR. J Am Chem Soc 1992;114:6291–6293.
37. Lohr F, Ruterjans H. A new triple-resonance experiment for the sequential assignment of backbone resonances in proteins. J Biomol NMR 2005;6:189–197.
38. Grzesiek S, Anglister J, Bax A. Correlation of backbone amide and aliphatic side-chain resonances in $^{13}C/^{15}N$-enriched proteins by isotropic mixing of carbon-13 magnetization. J Magn Reson 1993;101: 114–119.
39. Marion D, Driscoll PC, Kay LE, Wingfield PT, Bax A, Gronenborn AM, Clore GM. Overcoming the overlap problem in the assignment of ^{1}H NMR spectra of larger proteins by use of three-dimensional heteronuclear ^{1}H-^{15}N Hartmann-Hahn-multiple quantum coherence and nuclear Overhauser-multiple quantum coherence spectroscopy: application to interleukin 1β. Biochemistry 1989;28:6150–6156.
40. Kay LE, Xu GY, Singer AU, Muhandiram DR, Forman-Kay JD. A gradient-enhanced HCCH-TOCSY experiment for recording side-chain proton and carbon-13 correlations in water samples of proteins. J Magn Reson 1993;B101:333–337.
41. Yamazaki T, Forman-Kay JD, Kay LE. Two-dimensional NMR experiments for correlating $13C^{\beta}$ and $^{1}H^{\delta/\varepsilon}$ chemical shifts of aromatic residues in ^{13}C-labeled proteins via scalar couplings. J Am Chem Soc 1993;115:11054–11055.
42. Neri D, Szyperski T, Otting G, Senn H, Wuthrich K. Stereospecific nuclear magnetic resonance assignments of the methyl groups of valine and leucine in the DNA-binding domain of the 434 repressor by biosynthetically directed fractional ^{13}C labeling. Biochemistry 1989;28:7510–7516.
43. Marion D, Kay LE, Sparks SW, Torchia D, Bax A. Three-dimensional heteronuclear NMR of nitrogen-15 labeled proteins. J Am Chem Soc 1989;111:1515–1517.
44. Cornilescu G, Delaglio F, Bax A. Protein backbone angle restraints from searching a database for chemical shift and sequence homology. J Biomol NMR 1999;13:289–302.
45. Güntert P. Automated NMR structure calculation with CYANA. In: Downing AK, editor. Protein NMR techniques. Totowa, NJ: Humana Press; 2004. pp 353–378.
46. Herrmann T, Güntert P, Wüthrich K. Protein NMR structure determination with automated NOE assignment using the new software CANDID and the torsion angle dynamics algorithm DYANA. J Mol Biol 2002;319:209–227.
47. Laskowski RA, MacArthur MW, Moss DS, Thornton JM. PROCHECK: a program to check the stereochemical quality of protein structures. J Appl Crystallogr 1993;26:283–291.
48. Dosset P, Hus J-C, Blackledge M, Marion D. Efficient analysis of macromolecular rotational diffusion from heteronuclear relaxation data. J Biomol NMR 2000;16:23–28.
49. Tjandra N, Feller SE, Pastor RW, Bax A. Rotational diffusion anisotropy of human ubiquitin from ^{15}N NMR relaxation. J Am Chem Soc 1995;117:12562–12566.
50. Lipari G, Szabo A. Model-free approach to the interpretation of nuclear magnetic resonance relaxation in macromolecules. 1. Theory and range of validity. J Am Chem Soc 1982;104:4546–4559.
51. Lipari G, Szabo A. Model-free approach to the interpretation of nuclear magnetic resonance relaxation in macromolecules. 2. Analysis of experimental results J Am Chem Soc 1982;104:4559–4570.
52. Clore GM, Szabo A, Bax A, Kay LE, Driscoll PC, Gronenborn AM. Deviations from the simple two-parameter model-free approach to the interpretation of nitrogen-15 nuclear magnetic relaxation of proteins. J Am Chem Soc 1990;112:4989–4991.
53. Clore GM, Driscoll PC, Wingfield PT, Gronenborn AM. Analysis of the backbone dynamics of interleukin-1β using two-dimensional inverse detected heteronuclear ^{15}N-^{1}H NMR spectroscopy. Biochemistry 1990;29:7387–7401.
54. Mandel AM, Akke M, Palmer III AG. Backbone dynamics of *Escherichia coli* ribonuclease HI: correlations with structure and function in an active enzyme. J Mol Biol 1995;246:144–163.
55. DeLano WL. The PyMOL molecular graphics system, Version 1.3, Schrödinger, LLC. 2002.
56. Brunger AT, Adams PD, Clore GM, DeLano WL, Gros P, Grosse-Kunstleve RW, Jiang JS, Kuszewski J, Nilges M, Pannu NS, Read RJ, Rice LM, Simonson T, Warren GL. Crystallography & NMR system: a new software suite for macromolecular structure determination. Acta Crystallogr D Biol Crystallogr 1998;54:905–921.
57. Hubbard SJ, Thornton JM. NACCESS. London: Department of Biochemistry and Molecular Biology, University College London; 1993.
58. Krishnan VV, Cosman M. An empirical relationship between rotational correlation time and solvent accessible surface area. J Biomol NMR 1998;12:177–182.
59. Henzl MT, Wycoff WG, Larson JD, Likos JJ. ^{15}N nuclear magnetic resonance relaxation studies on rat β-parvalbumin and the pentacarboxylate variants, S55D and G98D, Protein Sci 2002;11: 158–173.
60. Henzl MT, Davis ME, Tan A. Leucine-85 is an important determinant of divalent ion affinity in rat β-parvalbumin (oncomodulin). Biochemistry 2008;47:13635–13646.
61. Schuermann JP, Tan A, Tanner JJ, Henzl MT. Structure of avian thymic hormone, a high-affinity avian β-parvalbumin, in the Ca^{2+}-free and Ca^{2+}-bound states. J Mol Biol 2010;397:991–1002.
62. Tan A, Henzl MT. Evidence for a Ca^{2+}-specific conformational change in avian thymic hormone, a high-affinity β-parvalbumin. Biochemistry 2009;48:3936–3945.
63. Henzl MT, Agah S, Larson JD. Association of the AB and CD-EF domains from rat α- and β-parvalbumin. Biochemistry 2004;43:10906–10917.